ACS APPLIED MATERIALS & INTERFACES

www.acsami.org

Research Article

Immunochromatographic Assay Based on Polydopamine-Decorated Iridium Oxide Nanoparticles for the Rapid Detection of Salbutamol in Food Samples

Shuang Zhao, Tong Bu, Kairong Yang, Zhihao Xu, Feier Bai, Kunyi He, Lihua Li, and Li Wang*

Cite This: *ACS Appl. Mater. Interfaces* 2021, 13, 28899−28907

Read Online

ACCESS | Metrics & More | Article Recommendations | Supporting Information

ABSTRACT: Salbutamol (SAL), a β-2 adrenoreceptor agonist, is an unpopular addition to livestock and poultry, causing several side effects to human health. Thus, it is very important to develop a simple and rapid analytical method to screen SAL in the field of food safety. Here, we present an immunochromatographic assay (ICA) method for sensitively detecting SAL with polydopamine-decorated iridium oxide nanoparticles (IrO_2@PDA NPs) as a signal tag. The IrO_2@PDA with excellent hydrophilicity, biocompatibility, and stability was synthesized by oxidating self-polymerization of dopamine hydrochloride (DAH) on the surface of IrO_2 NPs and used to label monoclonal antibodies (mAbs) through simple physical adsorption. Compared with IrO_2 NPs, the IrO_2@PDA also possessed superior optical properties and higher affinity with mAbs. With the proposed method, the limit of detection for SAL was 0.002 ng/mL, which was improved at least 24-fold and 180-fold compared with the IrO_2 NPs-based ICA and conventional gold nanoparticles-based ICA, respectively. Furthermore, the SAL residuals in pork, pork liver, and beef were successfully detected by the developed biosensor and the recoveries ranged from 85.56% to 115.56%. Briefly, this work indicated that the powerful IrO_2@PDA-based ICA can significantly improve detection sensitivity and has huge potential for accurate and sensitive detection of harmful small molecules analytes in food safety fields.

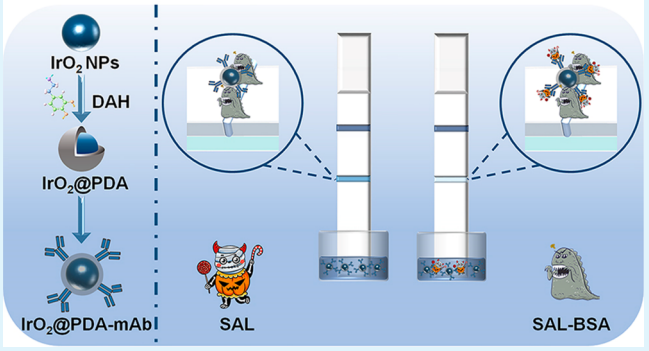

KEYWORDS: *salbutamol, immunochromatographic assay, iridium oxide nanoparticles, dopamine hydrochloride, sensitive*

1. INTRODUCTION

Salbutamol (SAL) is a quick acting β-2 adrenergic receptor agonist and is usually known as "lean meat powder", not only popularly used in the treatment of humans for chronic pulmonary disease and asthma, but also could increase lean meat-to-fat ratios of livestock.[1] In the breeding industry, when SAL doses are 5−10 times higher than the normal requirement of therapeutic treatment, it can sharply increase lean meat content and simultaneously decrease fat deposition, which can significantly enhance economic profit.[2] However, some studies have revealed that the residual SAL in animal tissue produced negative effects to human health, and caused some clinical symptoms such as heart palpitations, muscular tremors, dizziness, profuse sweating, and chills, etc.[3,4] Hence, SAL has been rigorously prohibited for use in animal husbandry by the Ministry Agriculture of China published Announcement No. 235 in 2002.[5] Thus, it is necessary to design a simple and rapid analytical method to screen SAL residues in animal tissues and meat-processing enterprises.

So far, various analytical techniques have been developed to monitor SAL in animal-derived foods including liquid chromatography tandem mass spectrometry (LC−MS/MS),[6,7] high performance liquid chromatography (HPLC),[8,9] gas chromatography−mass spectrometry (GC−MS),[10] enzyme-linked immunosorbent assay (ELISA),[11] surface enhanced Raman scattering (SERS),[1] and electrochemical detection.[12,13] Despite the fact that these conventional methods can provide highly sensitive detection and achieve accurate results, they require expensive instrumentation, professional operators, tedious sample-preprocessing steps, and time-consuming processes, which hinder their applications in the onsite and rapid detection.

Immunochromatographic assay (ICA) is widely used for fast monitoring in the food safety assessment field due to its simplicity, rapidity, sensitivity, and excellent selectivity.[14] It is noteworthy that the signal tag is an important factor affecting the expression and sensitivity of ICA.[15] Presently, gold nanoparticles (AuNPs) are a common signal tag owing to

Received: April 12, 2021
Accepted: June 2, 2021
Published: June 9, 2021

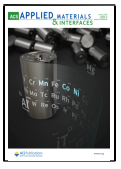

https://doi.org/10.1021/acsami.1c06724
ACS Appl. Mater. Interfaces 2021, 13, 28899−28907

their incomparable biocompatibility and unique optical properties.[16−20] Nonetheless, the low sensitivity of conventional AuNPs-ICAs severely impeded their further applications for low-level target detection.[21] Fortunately, due to their large surface area to volume ratio, high catalytic activity, and corrosion resistance, iridium oxide nanoparticles (IrO_2 NPs) are promising transition metal oxides that have been widely applied in electrocatalysis[22,23] and antitumor.[24] Furthermore, Quesada-Gonzalez et al. proved for the first time that IrO_2 NPs can be used on ICA to detect human immunoglobulin,[25] indicating that the IrO_2 NPs are expected to become an alternative signal label for AuNPs in ICA because of their simple synthesis method and excellent chemical stability. However, in the process of labeling monoclonal antibodies (mAbs), it is difficult to obtain a complete probe by high-speed centrifugation because the particle sizes of IrO_2 NPs are too small, resulting in the loss of a part of the mAbs. Therefore, it is necessary to explore a method to increase the particle size of IrO_2 NPs to avoid the wasting of mAbs in ICA application.

Dopamine hydrochloride (DAH), 3,4-dihydroxyphenethylamine, is an analog of L-DAH in mussel secretion adhesion protein. It oxidizes and self-polymerizes in a mild alkaline solution to form polydopamine (PDA).[26] In recent years, PDA has attracted notice due to its high chemical reactivity, good free radical quenching capacity, and strong adhesion property.[27] Thanks to the presence of abundant functional groups on the PDA surface such as catecholamine/chinone groups, the conformal coating can easily adhere onto the nanoparticles (NPs) surface via covalent linkage with amines or thiols, metal ion coordination, and electrostatic interactions.[28] Additionally, covering the surface of NPs with coating not only ensured the high affinity to various substrates, which could obviously enhance its hydrophilicity and biocompatibility, but at the same time, PDA also improves the color intensity of the NPs to facilitate test strip detection.[29] Briefly, these advantages of the PDA layer make the modified NPs have a broader perspective in many fields, including biomedical diagnosis and chemical analysis.

In this research, we synthesized IrO_2@PDA by oxidative self-polymerization on the surface of IrO_2 NPs with DAH and utilized it as a signal tag to construct an ICA biosensor, to detect SAL for the first time. IrO_2@PDA, with excellent hydrophilicity, biocompatibility, and stability, can quickly label monoclonal antibodies (mAbs) through simple physical adsorption, which subtly avoided using the complicated cross-linking agents. In addition, IrO_2@PDA possessed superior optical properties and higher affinity than IrO_2 NPs. Compared with IrO_2 NPs-ICA and traditional AuNPs-ICA, these advantages of IrO_2@PDA render it more suitable for application in ICA to significantly improve the sensitivity of detecting SAL. Furthermore, IrO_2@PDA-ICA was also applied in pork, pork liver, and beef samples to evaluate its reliability and practicability. Consequently, this work proves that the IrO_2@PDA-ICA has great potential for accurate and sensitive detection of small molecule analytes in food safety fields.

2. MATERIALS AND METHODS

2.1. Materials and Equipment. Potassium hexachloroiridate (K_2IrCl_6), trisodium citrate, sodium hydroxide (NaOH), sodium nitrite ($NaNO_2$), and 4-ethylcatechol (ECC) were purchased from Aladdin Co, Ltd. (Shanghai, China). Catechol (CC), 3,4-dimethoxyphenethylamine (DMPEA), and trichloroacetic acid were obtained from Sigma-Aldrich Chemical Co, Ltd. (St. Louis, MO). Melamine (MEL), ractopamine (RAC), clenbuterol (CLE), dopamine hydrochloride (DAH), chloramphenicol (CAP), streptomycin sulfate (STR), and salbutamol (SAL) (their chemical structures were displayed in Figure S1 of the Supporting Information, SI) were purchased from Macklin Biochemical Co., Ltd. (Shanghai, China). Goat antimouse IgG antibody, bovine serum albumin (BSA), SAL-BSA conjugates, and anti-SAL monoclonal antibodies (mAbs) were purchased from Shenzhen Baoankang Biotechnology Co., Ltd. (Shenzhen, China). Pork, pork liver, and beef samples were purchased from local supermarket (Xianyang, China). The nitrocellulose (NC) membrane, sample, conjugate, and absorbent pads were obtained by Shanghai Jinbiao Biological Technology Co., Ltd. (Shanghai, China).

The HGS-201 automatic programmable cutter, CSY-JA immunochromatographic test strip reader, and HGS510-5-1 biodot strip spray system were supplied by Fenghang Science Instrument Co, Ltd. (Zhejiang, China). Transmission electron microscopy (TEM) analyses were conducted to characterize the morphology of the synthesized particles (Tokyo, Japan). The Ultraviolet−visible (UV−vis) spectra were obtained from Shanghai Metash Instruments Co, Ltd. (Shanghai, China). The ζ-potentials of IrO_2 NPs and IrO_2@PDA were acquired from Malvern Panalytical Co. Ltd. (Malvern, U.K.).

2.2. Synthesis of IrO_2 NPs and IrO_2@PDA. The IrO_2 NPs were synthesized according to previously reported literature with minor modifications.[25] First, 50 mg trisodium citrate and 30 mg K_2IrCl_6 were mixed with 50 mL of ultrapure water and stirred for 5 min continuously. Then, the pH of the resulting solution was adjusted to 7.5 by using NaOH (0.25 M) and refluxed at boiling. When the color of the solution changed from brown to steel gray, continuing to stir the solution and heat for 30 min. After the solution was cooled to ambient temperature, the pH was readjusted to 7.5, and then the solution was heated for 30 min until pH was stable. The color of the final solution turned dark blue, indicating the formation of IrO_2 NPs. Finally, the IrO_2 NPs were stored in 4 °C. Color changes during the synthesis were shown in Figure S2.

The IrO_2 NPs synthesized above were decorated with DAH to form IrO_2@PDA. In short, 15 μL of 3% H_2O_2 was added to 1 mL of IrO_2 NPs and stirred for 10 min. Then 10 μL of DAH (10 mg/mL) was added to the above solution and stirred overnight. The precipitate of mixed solution was collected by centrifuging (9000 rpm, 30 min) and washed with ultrapure water twice. Finally, the purified IrO_2@PDA was suspended in ultrapure water and stored in 4 °C for further use.

2.3. Preparation of IrO_2@PDA-mAb Probe. The IrO_2@PDA was conjugated with mAbs via the electrostatic adsorption method. Briefly, 4 μg anti-SAL mAbs (1 mg/mL)was added into 1 mL of IrO_2@PDA solution and incubated for 60 min at 37 °C. After coupling, 100 μL of 10% BSA (w/v) solution was added to block the vacant sites on IrO_2@PDA. After blocking the reaction for 30 min, the unlabeled mAbs and BSA were discarded by centrifuging at 9000 rpm for 30 min. Finally, the precipitate was recovered and redispersed with 100 μL of 0.01 mol/L phosphate buffered solution (PBS). Similarly, the anti-SAL mAbs were conjugated with IrO_2 NPs and AuNPs, respectively.

2.4. Evaluation of the mAbs Performance of IrO_2 NPs and IrO_2@PDA. First, the mAbs coupling efficiencies of IrO_2 NPs and IrO_2@PDA were assessed. The standard curve of optical density at 450 nm (OD_{450}) relative to mAbs concentrations (1, 0.2, 0.1, 0.02, 0.004, and 0.001 μg/mL) was established by ELISA. Then, 1, 5, 10, 15, and 20 μg anti-SAL mAbs were added into 1 mL IrO_2@PDA and IrO_2 NPs solution. After centrifuging at 9000 rpm for 30 min to acquire the supernatant, then diluted 100 times to analyze the coupling efficiency of the mAbs. The coupling efficiency was calculated using the following equation:[29]

$$\text{coupling efficiency} = \frac{\text{total mAbs} - \text{supernatant mAbs}}{\text{total mAbs}} \times 100\% \quad (1)$$

Then, the mAbs affinity constant (k_a) and equilibrium dissociation constant (K_D) of IrO_2 NPs-mAb probe and IrO_2@PDA-mAb probe were also estimated. k_a represents the binding strength between

https://doi.org/10.1021/acsami.1c06724
ACS Appl. Mater. Interfaces 2021, 13, 28899−28907

Scheme 1. (A) The synthesis of the IrO_2@PDA and (B) the IrO_2@PDA-ICA for the Detection of SAL

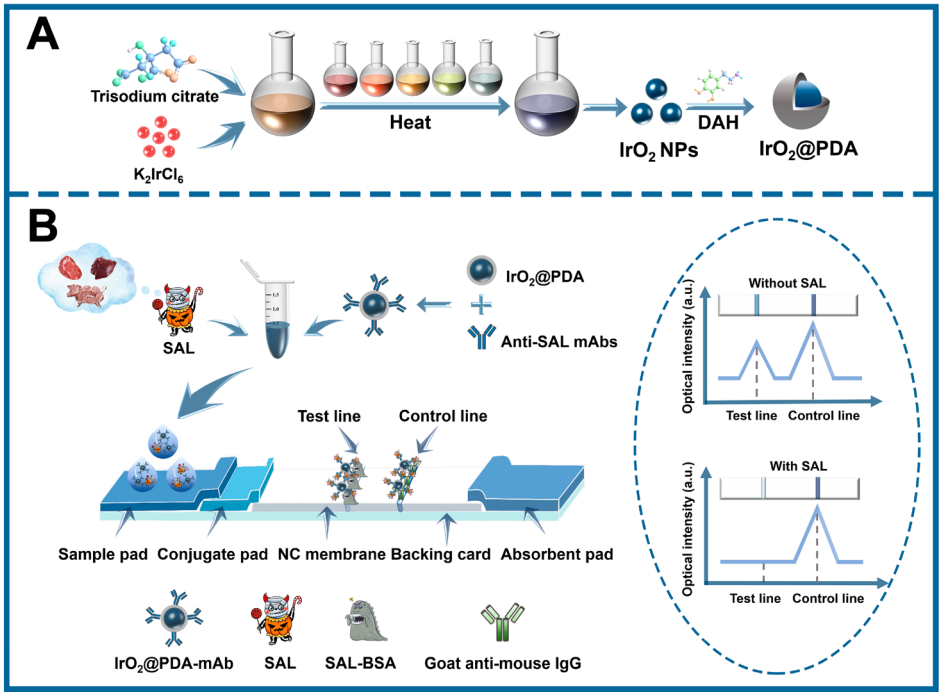

antigens and mAbs, which was measured by indirect competitive ELISA using the following equation:

$$k_a = \frac{n-1}{2(n[\mathrm{mAb}]_1 - [\mathrm{mAb}]_2)} \quad (2)$$

where n represents the multiple ratios of the two groups of coating antigen concentrations ($n > 1$), $[\mathrm{mAb}]_1$ and $[\mathrm{mAb}]_2$ represents the two mAbs concentrations corresponding to the absorbance signal at $OD_{max}/2$ in the two groups, respectively.

Moreover, according to the principle of Langmuir adsorption isotherm, the linearized equation of adsorption isotherm was used to estimate the dissociation constant (K_D):[30]

$$\frac{C}{\mathrm{Abs}} = \frac{C}{\mathrm{Abs(sat)}} + \frac{K_D}{\mathrm{Abs(sat)}} \quad (3)$$

where C represents the mAbs concentrations, Abs is the absorbance signal, and Abs(sat) is the absorbance signal at saturation.

2.5. Fabrication of the IrO_2@PDA-ICA. The ICA was composed of five components, namely, sample pad, conjugate pad, absorbent pad, NC membrane, and backing substrate. The sample and conjugate pads were soaked in 0.01 mol/L PBS solution containing 2% BSA and then dried at 37 °C for 8 h. The goat antimouse IgG (1 mg/mL) and SAL-BSA (1 mg/mL) were applied onto the NC membrane at different densities of 1 and 0.9 μL/cm as the control line (C-line) and test line (T-line), respectively. The distance between T and C lines were about 4 mm, then the prepared NC membrane was dried at 37 °C for 60 min. Afterward, different pads were assembled onto the backing substrate with an approximately 1−2 mm overlap and then were cut into 3 mm wide strip by automatic programmable cutter, and stored at 4 °C before use.

2.6. Assay Procedure and Evaluation of the IrO_2@PDA-ICA. The 100 μL various concentrations of SAL solution (0, 0.005, 0.01, 0.02, 0.045, 0.09, 0.18, 0.375, 0.75, 1.5, and 3 ng/mL) containing 2 μL of IrO_2@PDA-mAb probe were applied to the sample pad and migrated under the force of capillary action. Then, the optical intensity of the T-line was scanned with strip reader after reaction for 15 min. In this work, the limit of detection (LOD) was determined as the corresponding SAL concentration that caused a 10% inhibition of the T-line intensity by the IrO_2@PDA-ICA, it was calculated using the following four-parameter logarithmic equation:[31]

$$y = A_1 + \frac{A_1 - A_2}{1 + \left(\frac{x}{x_0}\right)^p} \quad (4)$$

where A_1 and A_2 are the asymptotic maximum (i.e., the T-line intensity in the absence of target analytes) and asymptotic minimum respectively, x_0 is equal to 50% inhibitory concentration (IC_{50}), and p is the curve slope at IC_{50}.

The specificity of the IrO_2@PDA-ICA was evaluated by analyzing SAL (0.75 ng/mL), as well as other food additives including MEL, RAC, CLE, CAP, STR, and $NaNO_2$ (100 ng/mL), respectively. Each experiment was repeated three times.

2.7. Analysis of SAL in Real Samples. To further investigate the reliability of IrO_2@PDA-ICA, pork, pork liver, and beef samples were selected as real samples. All samples were pretreated by an acid−base strategy. The chopped samples (5 g) were added into 10 mL of 3% trichloroacetic acid solution and thoroughly oscillated for 5 min. After centrifugation (10 000 rpm, 10 min), the pH of the acquired supernatant was adjusted to 7 by NaOH (1 M). Afterward, the resulting supernatant was diluted 10-fold with ultrapure water.

3. RESULTS AND DISCUSSION

3.1. Principle of IrO_2@PDA-ICA. Scheme 1 showed the principle of detecting SAL by IrO_2@PDA-based ICA biosensor. First, the IrO_2 NPs were synthesized by reducing K_2IrCl_6 with trisodium citrate under weakly alkaline conditions. Subsequently, the IrO_2@PDA was prepared by self-polymerization of DAH on the surface of IrO_2 NPs with DAH. The IrO_2@PDA exhibited excellent optical performance and high affinity with mAbs (Scheme 1A). As shown in Scheme 1B, the IrO_2@PDA-ICA was developed based on competitive immunoreaction. In the immunoassay, the sample solution and IrO_2@PDA-mAb probe were added onto the sample pad, then flowed through the strip by capillary action. For the negative sample, the IrO_2@PDA-mAb probe was recognized and captured by the specific antigen immobilized on the test line to form a visible band. For the positive sample, the probe was first combined with SAL and the remaining probe was captured by the T-line, so that the color intensity of T-line

https://doi.org/10.1021/acsami.1c06724
ACS Appl. Mater. Interfaces 2021, 13, 28899−28907

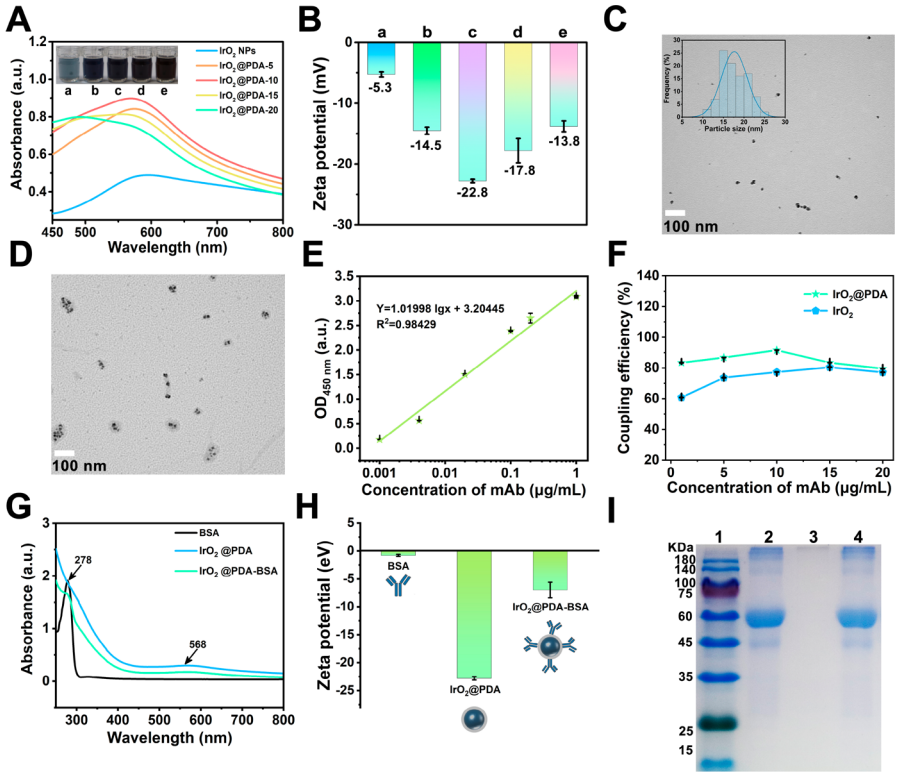

Figure 1. (A) UV−vis spectra and (B) ζ-potentials of (a) IrO_2 NPs, (b) IrO_2@PDA-5, (c) IrO_2@PDA-10, (d) IrO_2@PDA-15, and (e) IrO_2@PDA-20, respectively. TEM images of the prepared (C) IrO_2 NPs and (D) IrO_2@PDA. (E) Standard curve of OD_{450} relative to mAbs concentrations. (F) The mAbs coupling efficiencies of IrO_2 NPs and IrO_2@PDA. (G) UV−vis spectra, (H) ζ-potential, and (I) SDS-PAGE (1, 2, 3, and 4 represents Marker, BSA, IrO_2@PDA, and IrO_2@PDA-BSA, respectively) images of IrO_2 NPs and IrO_2@PDA-BSA.

was shallower than negative samples. When the SAL concentration reached high enough, the IrO_2@PDA-mAb probe was only captured on the C-line. Moreover, the results were observed with the naked eye and the T-line intensity was recorded with the strip reader for quantitative determination.

3.2. Optimization of the IrO_2@PDA Synthesis. Trisodium citrate is an important factor affecting the oxidative self-polymerizes of DAH on the surface of IrO_2 NPs. Therefore, we used different volumes of 3% H_2O_2 as an oxidant to oxidize sodium citrate. As revealed in Figure S3, the synthesized IrO_2@PDA had the highest absorbance when 15 μL of 3% H_2O_2 was added to the IrO_2 NPs solution. Since the reductive sodium citrate can inhibit the self-polymerization of DAH, the PDA layer will not be formed on the IrO_2 NPs without 3% H_2O_2. Therefore, 15 μL of 3% H_2O_2 was considered the optimal volume for further experiment. Furthermore, a series of structural analogs of DAH (DMPEA, CC, and ECC) were selected to coat IrO_2 NPs solution, and their absorbance was all lower than IrO_2 NPs + DAH (IrO_2@PDA), while pure DAH would not self-polymerize (Figure S4). Thus, DAH was selected for the following experiments. Subsequently, we optimized the amount of DAH added to the IrO_2 NPs solution. In the UV−vis spectra of Figure 1A, the maximum absorption peaks of the IrO_2@PDA-5, IrO_2@PDA-10, IrO_2@PDA-15, and IrO_2@PDA-20 were located at 575, 568, 556, and 494 nm when 5, 10, 15, and 20 μL DAH solution (10 mg/mL) were added, separately. Compared with the pure IrO_2 NPs solution, the self-polymerization of the PDA layer on the surface of IrO_2 NPs caused significant blue shift of the absorption peak. In addition, when 10 μL of DAH solution was added, the absorbance of IrO_2@PDA reached a maximum of 0.898. According to the Beer−Lambert law[32] ($\varepsilon = A/cl$, where ε is the molar absorptivity, A is the absorbance, c the concentration of sample, and l is the path length), the molar absorptivity of IrO_2@PDA-10 was at least 1.83-fold higher compared with that IrO_2 NPs solution. A thicker PDA coating was produced with the excessive volume of DAH solution, leading to IrO_2@PDA aggregation, so the absorbance decreased and a wider absorption peak was generated. Figure 1B showed that IrO_2 NPs, IrO_2@PDA-5, IrO_2@PDA-10, IrO_2@PDA-15, and IrO_2@PDA-20 had ζ-potentials of −5.3, −14.5, −22.8, −17.8, and −13.8 mV, respectively. The ζ-potential of DAH modified IrO_2 NPs was lower than that of pure IrO_2 NPs due to the abundance of −OH on the PDA coating. The ζ-potential indicated the stability of the nanodispersion. The absolute values of the ζ-potential in 0−10 mV, 10−20 mV, 20−30 mV, and above 30 mV were defined as extreme instability, relative stability, moderate stability, and high stability, respectively.[33] Thus, the IrO_2@PDA-10 was the most stable, which was selected as the signal label of ICA for the follow-up experiments.

3.3. Characterizations of the IrO_2@PDA and IrO_2@PDA-mAb Probe. As seen in the TEM image (Figure 1C), the synthesized IrO_2 NPs had excellent dispersity and uniformity, and the average size of 17.84 ± 2.99 nm. As TEM image of IrO2@PDA-10 shown in Figure 1D, the PDA layer was clearly adhered onto the IrO_2 NPs. A thicker PDA coating was produced with increasing DHA, while excessive volume of DAH led to IrO_2@PDA aggregation (Figure S5).

The mAbs coupling efficiencies of IrO_2 NPs and IrO_2@PDA were evaluated. Figure 1E was the standard curve of OD_{450}

https://doi.org/10.1021/acsami.1c06724
ACS Appl. Mater. Interfaces 2021, 13, 28899−28907

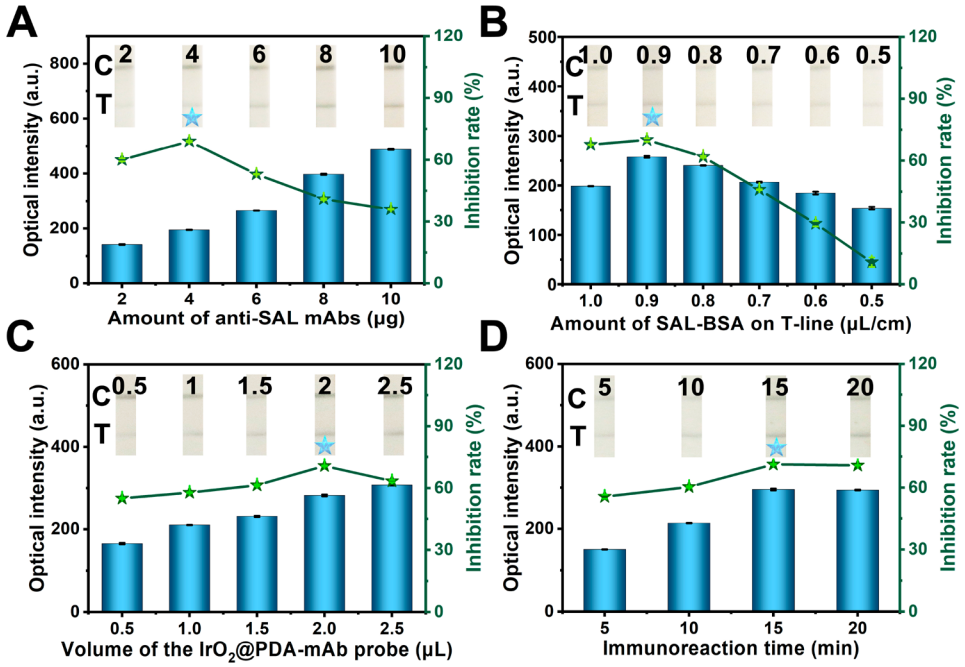

Figure 2. Effects of (A) amount of anti-SAL mAbs, (B) amount of SAL-BSA on T-line, (C) volume of the IrO_2@PDA-mAb probe, and (D) immunoreaction time on the IrO_2@PDA-ICA.

relative to mAbs concentrations (1, 0.2, 0.1, 0.02, 0.004, and 0.001 μg/mL). As displayed in Figure 1F, when the mAbs concentration was 10 μg/mL, the coupling efficiency of IrO_2@PDA reached the maximum of 91.56%, while the coupling efficiency of IrO_2 NPs reached the maximum of 80.43% when the mAbs concentration was 15 μg/mL. The above results indicated that IrO_2@PDA could significantly improve the coupling efficiency of mAbs compared with IrO_2 NPs. Moreover, we estimated the k_a value of IrO_2 NPs-mAb and IrO_2@PDA-mAb from indirect ELISA data respectively (Figure S6). The k_a of the IrO_2@PDA-mAb (7.595×10^8 M^{-1}) was at least 2-fold higher compared with that of IrO_2 NPs-mAb (3.179×10^8 M^{-1}). Meanwhile, the K_D value was also evaluated from the binding isotherm (Figure S7), the IrO_2@PDA-mAb (5.709×10^{-10} M) also showed a lower K_D value than the IrO_2 NPs-mAb (9.051×10^{-10} M). These results clearly indicated that the IrO_2@PDA possessed a high affinity with mAbs. The possible reason for the above results is that the quinone group in the PDA coating may participate in the nucleophilic addition reaction of $-SH$ and $-NH_2$ of the amino acid residues in the protein, resulting in more mAbs adsorbing on IrO_2@PDA.[34]

In order to further verify that the IrO_2@PDA could combine with proteins, the UV−vis spectra, ζ-potential, and sodium dodecyl sulfate polyacrylamide gel (SDS-PAGE) studies were performed. As displayed in Figure 1G, the UV−vis spectra of IrO_2@PDA-BSA showed a characteristic absorption peak of BSA (proteins) at 278 nm and an absorption peak of IrO_2@PDA at 568 nm. Moreover, in Figure 1H, compared with ζ-potential of IrO_2@PDA (−22.8 mV), the distinct change of ζ-potential of IrO_2@PDA-BSA (−6.97 mV) further demonstrated the electrostatic interaction between proteins and IrO_2@PDA. Besides, we found that the same blue band as BSA appeared at about 60 kDa in IrO_2@PDA-BSA, while no band was exhibited in the pure IrO_2@PDA (Figure 1I). On the basis of the above results, IrO_2@PDA can be effectively label proteins by electrostatic adsorption without any other modifications, averting the utilization of the complicated cross-linking agents.

3.4. Optimization of the IrO_2@PDA-ICA Conditions. In order to obtain the highest sensitivity of the IrO_2@PDA-ICA, different interaction conditions were optimized. To quantitatively detect SAL, "T-line intensity" and "inhibition rate" were used as the analysis standard for selecting the optimal conditions of the biosensor, and the inhibition rate was calculated by $(1 - T/T_0) \times 100\%$, where T_0 and T are T-line intensities of the negative samples and spiked samples analytes, respectively. In competitive immunoassay, the quantity of the mAbs was a key parameter, which directly affected the assay sensitivity of ICA, so the amount of anti-SAL mAbs was first optimized. In Figure 2A, T-line color intensity gradually enhanced with the amount of anti-SAL mAbs increasing. The inhibition ratio reached a maximal value when the amount of anti-SAL mAbs was 4 μg. For achieving higher sensitivity, 4 μg was regarded as the optimal mAbs quantity. The amount of SAL-BSA on T-line was also optimized in this work. As displayed in Figure 2B, the T-line color intensity decreased as the amount of SAL-BSA gradually decreased. After weighing up the T-line color intensity and inhibition ratio, 0.9 μL/cm was set as the optimal amount of SAL-BSA on T-line. In addition, as a recognition probe, the IrO_2@PDA-mAb usage amount could directly influence the signal intensity and sensitivity of ICA. As shown in Figure 2C, the inhibition ratio attained a maximum with 2 μL of the probe and then reduced after 2.5 μL. Thus, 2 μL of the probe was considered as the optimal volume for the following experiments. Figure 2D showed that the T-line intensity enhanced with a prolong immunoreaction time. The T-line intensity and inhibition rate reached a plateau at 15 min because the IrO_2@PDA-mAb probe was limited. Consequently, the optimum immunoreaction time for the detection of SAL by IrO_2@PDA-ICA was 15 min. Furthermore, the effect of different pH conditions on the detection of SAL were also investigated (Figure S8). The intensity of T-line was maximum when the pH value was 7.

https://doi.org/10.1021/acsami.1c06724
ACS Appl. Mater. Interfaces 2021, 13, 28899−28907

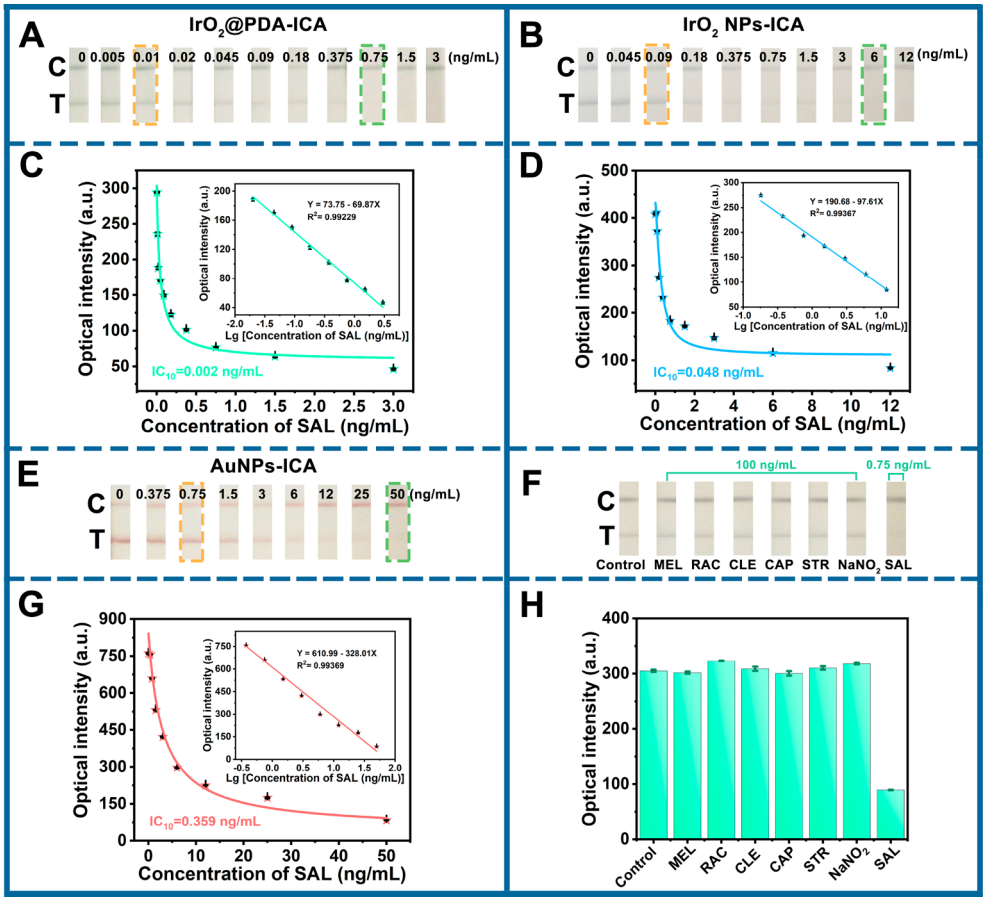

Figure 3. Photographs of detection of SAL by (A) IrO_2@PDA-ICA, (B) IrO_2 NPs-ICA, and (E) AuNPs-ICA. The variation rule in the whole detection range of the (C) IrO_2@PDA-ICA, (D) IrO_2 NPs-ICA, and (G) AuNPs-ICA with different concentrations of SAL. (Inset images: the calibration curves of SAL detection). The photographs (F) and the corresponding histogram (H) of specificity results of the IrO_2@PDA-ICA. SAL (0.75 ng/mL), other food additives (100 ng/mL).

Therefore, the pH value 7 for SAL could produce a satisfactory signal response. Other optimizations of IrO_2-mAb and AuNPs-mAb probes were shown in Figures S9 and S10.

3.5. Performance of the IrO_2@PDA-ICA. Under optimal experimental conditions, the detection capability of the IrO_2@PDA-ICA was evaluated with different concentrations of SAL standard solutions. The minimum target SAL concentration of color weaker on T-line than the blank control group was defined as the visual limit of detection (vLOD). When the color completely vanished on T-line, the minimum SAL concentration was represented as the cutoff value. As represented in (Figure 3A,B,E), the intensity of T-lines decreased as the concentrations of SAL increasing continuously. The results showed that the vLODs of IrO_2@PDA-ICA, IrO_2 NPs-ICA, and AuNPs-ICA for SAL detection were 0.01, 0.09, and 0.75 ng/mL, separately. And the cutoff values of SAL were 0.75, 6, and 50 ng/mL, respectively. In Figure 3C, a linear relationship between T-line intensity of IrO_2@PDA-ICA and the SAL concentrations was acquired in the dynamic range from 0.02 ng/mL to 3 ng/mL. The regression equation was described as $Y = 73.75-69.87X$ (X = Lg[SAL concentration]) with a linear regression coefficient (R^2) of 0.992. For the IrO_2 NPs-ICA, the regression equation in the dynamic range from 0.18 ng/mL to 12 ng/mL was described as $Y = 190.68-97.61X$ (X = Lg[SAL concentration]) with R^2 of 0.994 (Figure 3D). The IC_{10} value of IrO_2@PDA-ICA for SAL detection was calculated to be 0.002 ng/mL according to the standard curve, which was improved at least 24-fold and 180-fold compared with the IrO_2 NPs-ICA and the AuNPs-ICA, respectively. Furthermore, compared with previous reports (Table S1), our method has a decent sensitivity to detect SAL.

To investigate the specificity of the current immunoassay, different kinds of food additives that may have cross-reaction were tested, such as MEL, RAC, CLE, CAP, STR, and $NaNO_2$. As revealed in Figure 3F,H, only in the presence of SAL, the T-line color disappeared. In contrast, strong gray bands were observed on the T-line of other small molecules. Meanwhile, we verified the specificity of anti-SAL mAbs by a competitive ELISA (Figure S11), and the test results were consistent with IrO_2@PDA-ICA. The above results precisely manifested that the developed IrO_2@PDA-ICA has compelling specificity to detect SAL.

3.6. Analysis of SAL in Real Samples. Encouraged by the excellent sensitivity and selectivity of the IrO_2@PDA-ICA for SAL, we further evaluated its reliability and practicability. Different concentrations of spiked pork, pork liver, and beef samples (0.05−30 μg/kg) were selected as real samples to test SAL and analyzed of spiked-recovery. The intensity of T-line decreased gradually with the increasing of SAL concentration (Figure 4D). The cutoff values of SAL in pork, pork liver, and beef samples were all 7.5 μg/kg. The vLOD of pork and pork liver were 0.1 μg/kg, while it was 0.2 μg/kg in beef samples (Figure 4). Therefore, the matrix in beef samples had some interferences with the detection of SAL by IrO_2@PDA-ICA.

https://doi.org/10.1021/acsami.1c06724
ACS Appl. Mater. Interfaces 2021, 13, 28899−28907

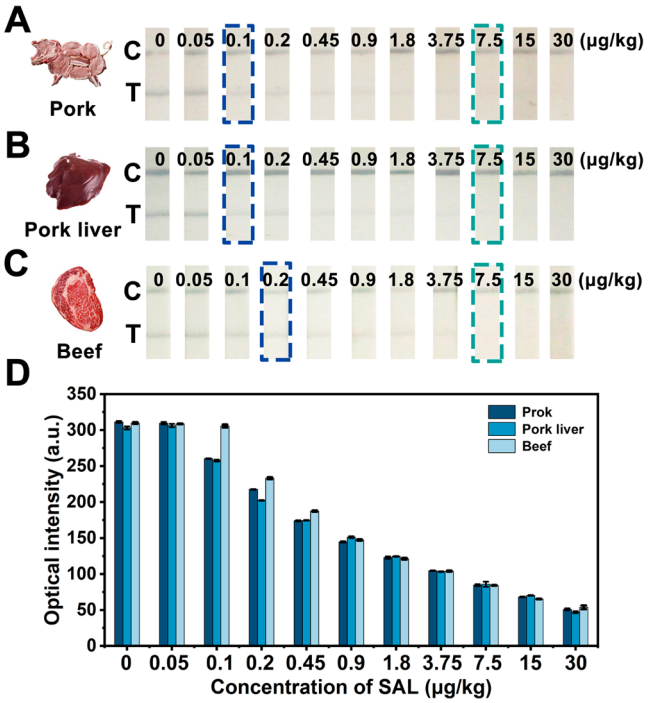

Figure 4. Detection results of SAL in (A) pork, (B) pork liver, and (C) beef samples by the IrO_2@PDA-ICA. (D) Relative intensity of T-line for various concentrations in real samples.

Furthermore, the spiked-recovery range of SAL was from 85.56% to 115.56% with relative standard deviation (RSD) values lower than 5.9% (Table 1). From these results, the developed system had the accuracy and feasibility for rapid screening of SAL in various sample matrixes after simple pretreatment.

4. CONCLUSIONS

In conclusion, the IrO_2@PDA was successfully synthesized and applied to ICA strips as a signal tag for sensitive detection of SAL. Owing to excellent hydrophilicity, biocompatibility, stability, bioaffinity, multiple active sites, and superb optical properties of IrO_2@PDA, the developed IrO_2@PDA-ICA exhibited outstanding sensitivity for SAL detection with a LOD of 0.002 ng/mL, which was improved at least 24-fold and 180-fold compared with the IrO_2 NPs-ICA and conventional AuNPs-ICA respectively. Concurrently, the proposed biosensor also exhibited compelling specificity for SAL detection. Furthermore, the IrO_2@PDA-ICA exhibited satisfactory applicability and reliability for the detection of SAL in pork, pork liver, and beef samples. Overall, the efficient, sensitive, and accurate biosensor provides a versatile and feasible platform for the on-site detection of harmful small molecules in the food samples. In future work, IrO_2 NPs can be integrated with other detection technologies[35] into ICA to achieve the detection of biomedical targets.

■ ASSOCIATED CONTENT

Supporting Information

The Supporting Information is available free of charge at https://pubs.acs.org/doi/10.1021/acsami.1c06724.

Preparation of traditional AuNPs; the immunological detection of SAL by ELISA; color changes during the IrO_2 NPs synthesis; effect of the volume of 3% H_2O_2 on the formation of IrO_2@PDA; TEM images of IrO_2@PDA; Affinity determination of IrO_2 NPs-mAb and IrO_2@PDA-mAb; optimization of the IrO_2 NPs-ICA and AuNPs-ICA conditions; specificity evaluation of the anti-SAL mAbs by ELISA; and comparison of the sensitivity for SAL detection by using different methods (PDF)

■ AUTHOR INFORMATION

Corresponding Author

Li Wang − *College of Food Science and Engineering, Northwest A&F University, Yangling 712100, Shaanxi, P. R. China;* orcid.org/0000-0003-3984-2494; Phone: +86 29-8709-2486; Email: lwang@nwsuaf.edu.cn; Fax: +86 29-8709-2486

Authors

Shuang Zhao − *College of Food Science and Engineering, Northwest A&F University, Yangling 712100, Shaanxi, P. R. China*

Tong Bu − *College of Food Science and Engineering, Northwest A&F University, Yangling 712100, Shaanxi, P. R. China*

Kairong Yang − *College of Food Science and Engineering, Northwest A&F University, Yangling 712100, Shaanxi, P. R. China*

Zhihao Xu − *College of Food Science and Engineering, Northwest A&F University, Yangling 712100, Shaanxi, P. R. China*

Feier Bai − *College of Food Science and Engineering, Northwest A&F University, Yangling 712100, Shaanxi, P. R. China*

Kunyi He − *College of Food Science and Engineering, Northwest A&F University, Yangling 712100, Shaanxi, P. R. China*

Table 1. Recovery Rates of SAL Spiked in Pork, Pork Liver, and Beef Samples Using IrO_2@PDA-ICA (n = 3)

sample	added (μg/kg)	found (μg/kg) ± SD	recovery (%) ± RSD (%)
pork	0.9	0.96 ± 0.03	106.67 ± 3.3
	1.8	1.97 ± 0.12	109.44 ± 5.9
	3.75	3.61 ± 0.05	96.26 ± 1.5
pork liver	0.9	0.77 ± 0.03	85.56 ± 3.5
	1.8	1.87 ± 0.03	103.89 ± 1.6
	3.75	3.77 ± 0.06	100.53 ± 1.6
beef	0.9	0.88 ± 0.03	97.78 ± 3.1
	1.8	2.08 ± 0.10	115.56 ± 4.7
	3.75	3.69 ± 0.09	98.41 ± 2.6

https://doi.org/10.1021/acsami.1c06724
ACS Appl. Mater. Interfaces 2021, 13, 28899−28907

Lihua Li − *College of Food Science and Engineering, Northwest A&F University, Yangling 712100, Shaanxi, P. R. China*

Complete contact information is available at: https://pubs.acs.org/10.1021/acsami.1c06724

Notes

The authors declare no competing financial interest.

■ ACKNOWLEDGMENTS

This work was supported by the Talented Program (A279021724) and the Fundamental Research Funds for the Northwest A&F University (No. Z111021601).

■ REFERENCES

(1) Cheng, J.; Su, X.-O.; Han, C.; Wang, S.; Wang, P.; Zhang, S.; Xie, J. Ultrasensitive detection of salbutamol in animal urine by immunomagnetic bead treatment coupling with surface-enhanced Raman spectroscopy. *Sens. Actuators, B* **2018**, *255*, 2329−2338.

(2) Zhao, L.; Zhou, H.; Sun, T.; Liu, W.; He, H.; Ning, B.; Li, S.; Peng, Y.; Han, D.; Zhao, Z.; Cui, J.; Gao, Z. Complete antigen-bridged DNA strand displacement amplification immuno-PCR assay for ultrasensitive detection of salbutamol. *Sci. Total Environ.* **2020**, *748*, 142330.

(3) Zhang, J.; Wei, Y.; Qiu, S.; Xiong, Y. A highly selective and simple fluorescent probe for salbutamol detection based on thioglycolic acid-capped CdTe quantum dots. *Spectrochim. Acta, Part A* **2021**, *247*, 119107.

(4) Rajaji, U.; Chinnapaiyan, S.; Chen, S. M.; Mani, G.; Alothman, A. A.; Alshgari, R. A. Bismuth telluride decorated on graphitic carbon nitrides based binary nanosheets: Its application in electrochemical determination of salbutamol (feed additive) in meat samples. *J. Hazard. Mater.* **2021**, *413*, 125265.

(5) Song, M.; Xiao, Z.; Xue, Y.; Zhang, X.; Ding, S.; Li, J. Development of an indirect competitive ELISA based on immunomagnetic beads' clean-up for detection of maduramicin in three chicken tissues. *Food Agric. Immunol.* **2018**, *29* (1), 590−599.

(6) Mastrianni, K. R.; Metavarayuth, K.; Brewer, W. E.; Wang, Q. Analysis of 10 beta-agonists in pork meat using automated dispersive pipette extraction and LC-MS/MS. *J. Chromatogr. B: Anal. Technol. Biomed. Life Sci.* **2018**, *1084*, 64−68.

(7) Chan, S. H.; Lee, W.; Asmawi, M. Z.; Tan, S. C. Chiral liquid chromatography-mass spectrometry (LC-MS/MS) method development for the detection of salbutamol in urine samples. *J. Chromatogr. B: Anal. Technol. Biomed. Life Sci.* **2016**, *1025*, 83−91.

(8) Yan, H.; Wang, R.; Han, Y.; Liu, S. Screening, recognition and quantitation of salbutamol residues in ham sausages by molecularly imprinted solid phase extraction coupled with high-performance liquid chromatography-ultraviolet detection. *J. Chromatogr. B: Anal. Technol. Biomed. Life Sci.* **2012**, *900*, 18−23.

(9) Tamisierkarolak, L.; Delhotallandes, B.; Jollietriant, P.; Milliez, J.; Jannet, D.; Barre, J.; Flouvat, B. Plasma assay of salbutamol by means of high-performance liquid-chromatography with amperometric determination using a loop column for injection of plasma extracts-application to the evaluation of subcutaneous administration of salbutamol. *Ther. Drug Monit.* **1992**, *14* (3), 243−248.

(10) Cordell, R. L.; Valkenburg, T. S. E.; Pandya, H. C.; Hawcutt, D. B.; Semple, M. G.; Monks, P. S. Quantitation of salbutamol using micro-volume blood sampling − applications to exacerbations of pediatric asthma. *J. Asthma* **2018**, *55* (11), 1205−1213.

(11) He, H.; Sun, T.; Liu, W.; Xu, Z.; Han, Z.; Zhao, L.; Wu, X.; Ning, B.; Bai, J. Highly sensitive detection of salbutamol by ALP-mediated plasmonic ELISA based on controlled growth of AgNPs. *Microchem. J.* **2020**, *156*, 104804.

(12) Zhang, J.; Cai, F.; Deng, A.; Li, J. CdSe quantum dots based electrochemiluminescence immunosensor with simple structure for ultrasensitive detection of salbutamol. *Electroanalysis* **2014**, *26* (4), 873−881.

(13) Chen, D.; Yang, M.; Zheng, N.; Xie, N.; Liu, D.; Xie, C.; Yao, D. A novel aptasensor for electrochemical detection of ractopamine, clenbuterol, salbutamol, phenylethanolamine and procaterol. *Biosens. Bioelectron.* **2016**, *80*, 525−531.

(14) Bu, T.; Zhang, M.; Sun, X.; Tian, Y.; Bai, F.; Jia, P.; Bai, Y.; Zhe, T.; Wang, L. Gold nanoparticles-functionalized microorganisms assisted construction of immunobiosensor for sensitive detection of ochratoxin A in food samples. *Sens. Actuators, B* **2019**, *299*, 126969.

(15) Su, L.; Wang, L.; Yao, X.; Yin, X.; Zhang, H.; Zhao, M.; Liu, S.; Wang, Z.; Wang, J.; Zhang, D. Small size nanoparticles-Co_3O_4 based lateral flow immunoassay biosensor for highly sensitive and rapid detection of furazolidone. *Talanta* **2020**, *211*, 120729.

(16) Zvereva, E. A.; Zherdev, A. V.; Xu, C.; Dzantiev, B. B. Highly sensitive immunochromatographic assay for qualitative and quantitative control of beta-agonist salbutamol and its structural analogs in foods. *Food Control* **2018**, *86*, 50−58.

(17) Chen, Y.; Guo, L.; Liu, L.; Song, S.; Kuang, H.; Xu, C. Ultrasensitive immunochromatographic strip for fast screening of 27 sulfonamides in honey and pork liver samples based on a monoclonal antibody. *J. Agric. Food Chem.* **2017**, *65* (37), 8248−8255.

(18) Khamta, Y.; Pattarawarapan, M.; Nangola, S.; Tayapiwatana, C. Development of immunochromatographic assay for the on-site detection of salbutamol. *J. Immunoassay Immunochem.* **2009**, *30* (4), 441−456.

(19) Liu, R.; Liu, L.; Song, S.; Cui, G.; Zheng, Q.; Kuang, H.; Xu, C. Development of an immunochromatographic strip for the rapid detection of 10 β-agonists based on an ultrasensitive monoclonal antibody. *Food Agric. Immunol.* **2017**, *28* (4), 625−638.

(20) Baniukevic, J.; Hakki Boyaci, I.; Goktug Bozkurt, A.; Tamer, U.; Ramanavicius, A.; Ramanaviciene, A. Magnetic gold nanoparticles in SERS-based sandwich immunoassay for antigen detection by well oriented antibodies. *Biosens. Bioelectron.* **2013**, *43*, 281−288.

(21) Zhao, S.; Bu, T.; He, K.; Bai, F.; Zhang, M.; Tian, Y.; Sun, X.; Wang, X.; Zhangsun, H.; Wang, L. A novel α-Fe_2O_3 nanocubes-based multiplex immunochromatographic assay for simultaneous detection of deoxynivalenol and aflatoxin B_1 in food samples. *Food Control* **2021**, *123*, 107811.

(22) Lim, J.; Park, D.; Jeon, S. S.; Roh, C.-W.; Choi, J.; Yoon, D.; Park, M.; Jung, H.; Lee, H. Ultrathin IrO_2 nanoneedles for electrochemical water oxidation. *Adv. Funct. Mater.* **2018**, *28* (4), 1704796.

(23) Ma, Y.; Yang, J.; Yang, T.; Deng, Y.; Gu, M.; Wang, M.; Hu, R.; Yang, Y. Electrochemical detection of C-reactive protein using functionalized iridium nanoparticles/graphene oxide as a tag. *RSC Adv.* **2020**, *10* (16), 9723−9729.

(24) Zhen, W.; Liu, Y.; Lin, L.; Bai, J.; Jia, X.; Tian, H.; Jiang, X. BSA-IrO_2: Catalase-like nanoparticles with high photothermal conversion efficiency and a high X-ray absorption coefficient for anti-inflammation and antitumor theranostics. *Angew. Chem., Int. Ed.* **2018**, *57* (32), 10309−10313.

(25) Quesada-Gonzalez, D.; Sena-Torralba, A.; Wicaksono, W. P.; de la Escosura-Muniz, A.; Ivandini, T. A.; Merkoci, A. Iridium oxide (IV) nanoparticle-based lateral flow immunoassay. *Biosens. Bioelectron.* **2019**, *132*, 132−135.

(26) Jung, H. S.; Cho, K. J.; Seol, Y.; Takagi, Y.; Dittmore, A.; Roche, P. A.; Neuman, K. C. Polydopamine encapsulation of fluorescent nanodiamonds for biomedical applications. *Adv. Funct. Mater.* **2018**, *28* (33), 1801252.

(27) Amin, D. R.; Higginson, C. J.; Korpusik, A. B.; Gonthier, A. R.; Messersmith, P. B. Untemplated resveratrol-mediated polydopamine nanocapsule formation. *ACS Appl. Mater. Interfaces* **2018**, *10* (40), 34792−34801.

(28) Wang, Z.; Zou, Y.; Li, Y.; Cheng, Y. Metal-containing polydopamine nanomaterials: catalysis, energy, and theranostics. *Small* **2020**, *16* (18), 1907042.

(29) Xu, S.; Zhang, G.; Fang, B.; Xiong, Q.; Duan, H.; Lai, W. Lateral flow immunoassay based on polydopamine-coated gold nanoparticles for the sensitive detection of zearalenone in maize. *ACS Appl. Mater. Interfaces* **2019**, *11* (34), 31283−31290.

(30) Lee, E. J.; Lee, E.; Kim, H. J.; Lee, J. H.; Ahn, K. Y.; Park, J. S.; Lee, J. Self-assembled proteinticle nanostructures for 3-dimensional display of antibodies. *Nanoscale* **2014**, *6* (24), 14919−14925.
(31) Qie, Z.; Liu, Q.; Yan, W.; Gao, Z.; Meng, W.; Xiao, R.; Wang, S. Universal and ultrasensitive immunochromatographic assay by using an antigen as a bifunctional element and antialbumin antibody on a test line. *Anal. Chem.* **2019**, *91* (15), 9530−9537.
(32) Duarte, A. R. C.; Anderson, L. E.; Duarte, C. M. M.; Kazarian, S. G. A comparison between gravimetric and in situ spectroscopic methods to measure the sorption of CO_2 in a biocompatible polymer. *J. Supercrit. Fluids* **2005**, *36* (2), 160−165.
(33) Lai, X.; Zhang, G.; Zeng, L.; Xiao, X.; Peng, J.; Guo, P.; Zhang, W.; Lai, W. Synthesis of PDA-mediated magnetic bimetallic nanozyme and its application in immunochromatographic assay. *ACS Appl. Mater. Interfaces* **2021**, *13* (1), 1413−1423.
(34) Sureshkumar, M.; Lee, C.-K. Polydopamine coated magnetic-chitin (MCT) particles as a new matrix for enzyme immobilization. *Carbohydr. Polym.* **2011**, *84* (2), 775−780.
(35) Drobysh, M.; Ramanaviciene, A.; Viter, R.; Ramanavicius, A. Affinity sensors for the diagnosis of COVID-19. *Micromachines (Basel)* **2021**, *12* (4), 390.

https://doi.org/10.1021/acsami.1c06724
ACS Appl. Mater. Interfaces 2021, 13, 28899−28907